

Article

Characterization of Chromophoric Dissolved Organic Matter in the Littoral Zones of Eutrophic Lakes Taihu and Hongze during the Algal Bloom Season

Bingfa Chen ^{1,2}, Wei Huang ¹, Shuzhan Ma ^{1,2}, Muhua Feng ¹, Cheng Liu ¹ , Xiaozhi Gu ¹ and Kaining Chen ^{1,*}

¹ State Key Laboratory of Lake Science and Environment, Nanjing Institute of Geography and Limnology, Chinese Academy of Sciences, Nanjing 210008, China; cbingfa@126.com (B.C.); amwuanff@163.com (W.H.); mashuzhanfan@126.com (S.M.); mhfang@niglas.ac.cn (M.F.); chliu@niglas.ac.cn (C.L.); guxiaozhi@163.com (X.G.)

² University of Chinese Academy of Sciences, Beijing 100049, China

* Correspondence: knchen@niglas.ac.cn; Tel.: +86-25-8688-2216

Received: 27 May 2018; Accepted: 23 June 2018; Published: 28 June 2018



Abstract: Chromophoric dissolved organic matter (CDOM) is a key component with a critical role in the littoral zones of eutrophic shallow lakes; yet the characteristics of CDOM in these zones remain seldom systematically reported. In this study, the differences in sources, biogeochemical characteristics, and fates of CDOM between the littoral zones of eutrophic lakes Taihu (LLT; frequently occurring algal blooms and longer lake residence time) and Hongze (LLH; no obvious algal blooms and shorter residence time) were compared during the algal bloom season using ultraviolet-visible spectra and excitation and emission matrix spectroscopy combined with parallel factor analysis. Three humic-like fluorescent dissolved organic matter (FDOM) components (C1, C3, and C4) and one protein-like component (C2) were identified. Results showed that FDOM components were dominated by protein-like fluorescent substances in LLT, and humic-like materials in LLH, respectively. The CDOM in LLT had a lower relative aromaticity and molecular weight, humification degree and a higher autotrophic productivity because of algal blooms. Furthermore, CDOM depletion rates in LLT were higher than those in LLH due to a longer lake residence time in LLT. In addition, CDOM shifted from high molecular weight to low molecular weight as the humification degree decreased during the CDOM depletion process. This comparative study showed that algal blooms and lake residence time were the significant factors for distinguishing characteristics of CDOM between littoral zones of shallow lakes on a similar trophic level. This study provides field-based knowledge for remote sensing CDOM measurement and serves as a reference for lakeshore aquatic environmental management.

Keywords: chromophoric dissolved organic matter; excitation emission matrix spectroscopy; littoral zone; eutrophic lake

1. Introduction

Chromophoric dissolved organic matter (CDOM), the colored fraction of dissolved organic matter (DOM), consisting of aromatics, carbohydrates, and humic, fulvic and proteinaceous materials, is an optically active substance in the water column that plays a momentous role in lake ecosystems [1–3]. It affects the underwater light field [4], carbon and nutrient cycling [5], metal migration and transformation [6], and contaminant biotoxicity [7] in lakes and the drinking water treatment distributed along a lakeside [8]. It can be also used as a rapid environmental indication of lake

trophic states and for remote-sensing estimations of total suspended matter concentrations [9,10]. Therefore, it is essential to understand the abundances, sources, and dynamics of CDOM in eutrophic lakes for water quality management and ecological protection.

Generally, CDOM is a complicated mixture of organic matter, making it arduous to identify all chemical compositions [11]. Fortunately, optical indicative information by means of ultraviolet-visible (UV-Vis) absorption spectroscopy and excitation-emission matrix fluorescence spectroscopy (EEMs) has been widely applied and provide more insight into CDOM fractions and their chemical characteristics because the methods are sensitive, timesaving, informative and require a small sample volume [11–13]. Furthermore, a mathematical modeling approach termed parallel factor analysis (PARAFAC) was applied to decompose EEMs data into individual fluorescent components, and this solved the overlapping signals of various types of fluorophores [14,15]. Over the past decades, littoral zones of eutrophic shallow lakes have been strongly affected by anthropogenic activities and have become enrichment regions of dissolved organic matter with extremely active mineralization, all of which result in a significant influence on material circulation of lake ecosystems [16–18]. Furthermore, the sources and dynamics of CDOM in littoral zones are complex; research on the compositions and transformations of CDOM in littoral zones is indispensable and meaningful for obtaining a clear understanding of the biogeochemical characteristics of dissolved organic matter in lake ecosystems. To date, structural characteristics of CDOM and spatial changes in the littoral zones of eutrophic shallow lakes remain seldom systematically reported. Obviously, targeted sampling and studies are required in the littoral zones of eutrophic shallow lakes.

Therefore, in this study, we compared the characteristics of CDOM in littoral zones of Lake Taihu (LLT) and Lake Hongze (LLH), the third- and fourth-largest freshwater lakes in the middle and lower reaches of the Yangtze River of China, with different cyanobacterial bloom frequencies and water retention times, during the algal bloom season using UV-Vis absorbance and EEMs spectra [19]. PARAFAC analysis was also conducted to identify the major fluorescent CDOM components. The primary objective was to compare the differences in CDOM characteristics between LLT and LLH during the algal bloom season, including information on the sources, biogeochemical characteristics, and fates of the CDOM in the interior of LLT and LLH.

2. Materials and Methods

2.1. Study Area

Lake Taihu and Lake Hongze have an area and mean water depth of 2338 km² and 2.1 m, 1597 km² and 1.9 m, respectively [19,20]. Although the surface area of Lake Taihu is larger than that of Lake Hongze, the drainage area of Lake Hongze (15.87×10^4 km²) is 4.28-times larger than that of Lake Taihu (3.65×10^4 km²). Meanwhile, the water retention time in Lake Taihu (309 d) is approximately 9-times longer than that of Lake Hongze (35 d) [20–22]. These two shallow lakes have already evolved into a eutrophic state as a result of anthropogenic activities [20]. During recent years, Lake Taihu has frequently been subject to severe cyanobacterial blooms, particularly in the northern and northwestern littoral zones during summer, whereas the intensity and frequency of blooms in Lake Hongze has been far less than those in Lake Taihu [23,24]. In addition, the southeastern littoral zone of Lake Taihu and the northern zone of Lake Hongze are distinguished by large areas of aquatic macrophytes [25,26]. We hypothesized that there were significant differences in the CDOM characteristics between the littoral zones of these two eutrophic lakes with different cyanobacterial bloom frequencies and water retention times, particularly during the algal bloom season.

2.2. Sample Collection

Water samples from LLT and LLH were collected from 10–14 August 2017 ($n = 91$) and 18–20 August 2017 ($n = 52$), respectively. This period was the most serious algal bloom season in the middle and lower reaches of the Yangtze River. To compare the interior structure and abundance

of CDOM on the lakeshore based on the influence of inflowing and outflowing river and water flow direction in each lake, LLT was divided into a major-inflowing-river-influenced zone with serious cyanobacterial blooms (upstream, Tin group) and a major outflowing-river-connected and aquatic-macrophyte-dominated zone (downstream, Tout group). LLH was also divided into an upstream (Hin group) and downstream (Hout group) according to the inflowing and outflowing river influences. There is a sporadic distribution of aquatic macrophytes in Hin and Hout. Moreover, the north part of LLH, less affected by rivers and dominated by aquatic macrophytes, was divided into the Hmac group (Figure 1).

Surface water (0.5–1 m below the surface) samples were collected in 1-L, acid-cleaned polyethylene bottles and stored in an ice box while in the field. Within 2 h after collection, the samples were transported to the laboratory where they were immediately filtered and stored in the dark at $-20\text{ }^{\circ}\text{C}$. CDOM optical measurements and nutrient determinations were completed within one week.

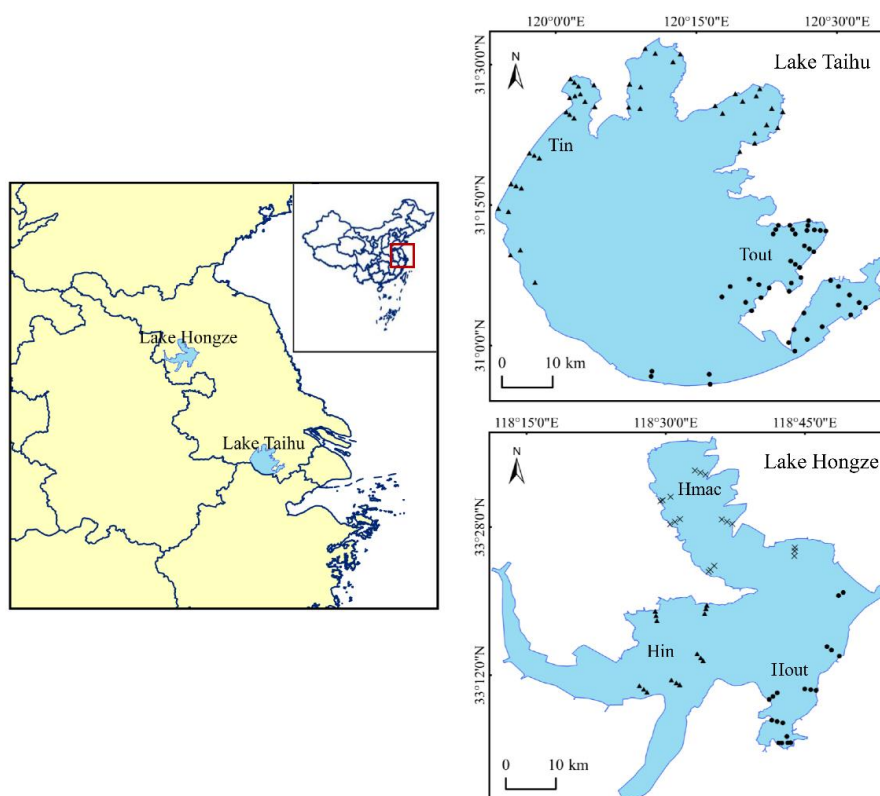


Figure 1. Locations of the sampling sites and different sections in littoral zones of Lakes Taihu and Hongze in August 2017. The inflowing-river-affected zones (filled triangles, Tin and Hin), the outflowing-river-connected zones (filled circles, Tout and Hout), and lightly-affected by rivers and aquatic macrophyte-dominated zone (furcation, Hmac).

2.3. CDOM Absorption and Fluorescence Measurements

Samples were filtered at low pressure using a pre-combusted ($550\text{ }^{\circ}\text{C}$ for 6 h) Whatman GF/F filter ($0.7\text{ }\mu\text{m}$). Part of the 30 mL filtrates for dissolved organic carbon (DOC) detection were poured into pre-combusted ($550\text{ }^{\circ}\text{C}$ for 6 h) brown glass bottles; the remaining part was then transferred into a Millipore mixed cellulose esters membrane ($0.22\text{ }\mu\text{m}$) in glass bottles identical to those previously mentioned to detect CDOM absorption and fluorescence spectra. It should be noted that the first 10–20 mL of filtrates were discarded to rinse the Millipore membrane and filter flask.

The absorption spectra were obtained between 200 nm and 800 nm at 1-nm intervals, using a Shimadzu UV-2700 UV-Vis recording spectrophotometer with 1-cm quartz cells. Milli-Q water was used as a reference. Absorbance spectra were corrected by subtracting the mean absorbance from

700 nm to 800 nm. Absorption coefficients were obtained by multiplying the absorbance by $2.303/L$, where L is the cuvette path length in m. In this study, the relative concentration of CDOM was expressed using $a(350)$, which has been widely used in various aquatic ecosystems [27,28].

The spectral slope of the CDOM absorption curve (S) was calculated by nonlinear regression according to the equation of Markager and Vincent [29]. The spectral slope ratio (S_R) of two wavelength ranges (275–295 nm and 350–400 nm) was used to indicate the microbial activities and sources of CDOM. We also applied M (the ratio of CDOM absorption at 250 nm to 365 nm) and $S_{275-295}$ to estimate relative molecular size variations in which the relative molecular size of CDOM increases as the M and $S_{275-295}$ decreases [13]. These two optical parameters have also been applied in our research systems or similar systems in previous studies [17,30,31].

The EEMs spectra of CDOM were measured using a HORIBA Fluorolog-3 spectrofluorometer with a 450-W xenon lamp and CCD detector. The scanning ranges used were 250–450 nm for excitation in 5-nm intervals, and 250–580 nm for emission in 1-nm intervals, with a 0.2-s integration time and 5-nm slit width on the excitation and emission monochromators. EEMs data were corrected for instrumental differences using Fluorolog Operation manual correction factors. Blank EEMs and Raman scans ($\lambda_{ex} = 350$ nm, $\lambda_{em} = 360$ –450 nm at 1-nm intervals) of Milli-Q water were also collected [32]. Inner-filter effects correction and Rayleigh scatter exclusion were run using the decomposition routines for excitation emission matrices (drEEM) toolbox [15]. Daily lamp variations were accounted by normalizing fluorescence to the integral of the Raman signal (excitation 350 nm) [33].

The humification index (HIX) was obtained from the ratio of the integration of fluorescence between the 300–345 nm and 435–480 nm wavelengths over excitation at 254 nm [34]. The biological index (BIX) was calculated as the ratio of fluorescence intensity at 380 nm to that at 430 nm under the excitation wavelength of 310 nm; higher values of HIX were related to a higher molecular weight aromaticity and humification, a low percentage of oxygen-containing functional groups for terrestrially derived CDOM, and high values of BIX (>1) corresponding to a mainly autochthonous origin of CDOM and the presence of OM freshly released into water; higher values of BIX indicates higher autotrophic productivity [35–37].

2.4. Parallel Factor Analysis Modeling

PARAFAC is an alternating least-squares algorithm applicable to data that are arranged in three- or higher-order arrays [15]. PARAFAC modeling was conducted in MATLAB software (R2012a) using the drEEM and N-way toolbox [15,38]. The EEMs data array consisted of 143 samples with 330 emission wavelengths and 40 excitation wavelengths. To validate the model, split half analysis was performed to determine the optimal components before guaranteeing the removal of outliers and developing preliminary models. In this study, we assembled six different datasets ‘halves’ and produced three validation tests ‘S4C6T3’ as referred to Murphy et al. [15]. Four components were well-validated by split-half analysis, and the output parameters, including the sum of squares of the residuals and the explained variation of the model, suggested that a four-component model explained more than 99% of the total EEMs variables, the maximal fluorescent intensity (F_{max}) of individual fluorescent component was used to represent the real concentrations of the corresponding fractions of fluorescent dissolved organic matter (FDOM) [30]. In order to set forth the degree of CDOM loss from upstream zones to downstream zones during lake water translocation processes, the CDOM depletion rates were estimated based on loss ratios in mean values of $a(350)$ or F_{max} from upstream zones to downstream zones [3].

2.5. Other Water Quality Parameters

Concentrations of DOC were measured using a Shimadzu TOC-V CPN analyzer and the high temperature combustion method. Samples for Chlorophyll a (Chla) were filtered onto Whatman glass fiber GF/C filters (\varnothing 47 mm) and the Chla was extracted using 90% acetone at 4 °C and analyzed at varying wavelengths using a Shimadzu UV-2700 UV-Vis spectrophotometer [39]. Secchi depth

was obtained using a Secchi disk. Total nitrogen (TN) and total phosphorus (TP) were determined by a combined persulfate digestion, followed by spectrophotometric analysis for soluble reactive phosphorus (SRP) and nitrate nitrogen (NO_3^- -N) [40].

2.6. Statistical Analyses

Statistical analyses, including mean values, standard deviation (SD), *t*-tests, standard deviations, and linear and non-linear fitting were performed using SPSS 18.0 and Origin 8.5 software. Spatial mapping of sampling sites and the CDOM-related parameter distribution were completed using ArcGIS 10.5 and MATLAB 2012a software. Significance levels were reported as non-significant (NS) ($p > 0.05$), significant ($0.01 < p < 0.05$), or highly significant ($p < 0.01$).

3. Results

3.1. Characteristics of Water Quality Parameters

The values of the nutrients, Chla and DOC in the water samples collecting from LLT and LLH and the corresponding spatial sections are presented in Table 1. The results show that there were significant differences in TP concentrations ($p < 0.01$) between the two lakeshore zones; nevertheless there were no obvious differences in TN concentrations ($p = 0.44$, NS). The DOC concentrations of all sampling sites at LLT and LLH ranged from 2.41 to 13.29 mg/L and 3.92 to 17.33 mg/L, respectively. There were no significant differences in the corresponding spatial sections of LLT and LLH ($p = 0.09$, NS). The averaged value of the Chla concentrations of all the sampled sites in LLT was 51.06 ± 47.45 $\mu\text{g/L}$, significantly higher than the 29.93 ± 28.23 $\mu\text{g/L}$ in LLH ($p < 0.05$). Spatially, the results showed that the mean Chla value in Tin was much higher than that in Tout ($p < 0.01$), whereas the Chla values of Hin and Hmac were much lower than that of Hout ($p < 0.01$). The mean values of Secchi depth in LLT were higher than those of LLH, but no significant differences were found ($p = 0.36$, NS). According to the Organization for Economic Cooperation and Development (OECD) criteria, using the variables of TP, TN, Chla, and Secchi depth to evaluate trophic status, the limits of values of variables in the hypereutrophic state were mean TP > 0.1 mg/L, mean Chla > 25 $\mu\text{g/L}$, max Chla > 75 $\mu\text{g/L}$, mean Secchi depth < 1.5 m and min Secchi depth < 0.7 m [41]. LLT and LLH were both hypereutrophic during the sampling period.

3.2. UV-Vis Spectral Parameter Characteristics and Spatial Distribution

The S_R values of both LLT and LLH were all near 1 (Table 1), although statistical differences were found via the *t*-test ($p < 0.05$). The values of M and $S_{275-295}$ in LLT were statistically higher than those in LLH ($p < 0.05$) (Table 1). The absorption coefficients of CDOM at 350 nm ranged from 1.40 m^{-1} to 5.96 m^{-1} with a mean value of 3.27 ± 1.33 m^{-1} in LLT and from 2.61 m^{-1} to 7.49 m^{-1} with a mean value of 4.57 ± 1.31 m^{-1} in LLH. The $a(350)$ in LLH was significantly higher than that in LLT ($p < 0.01$) (Figure 2).

Furthermore, spatially, $a(350)$ was much higher in the Tin group than that in the Tout section, and $a(350)$ was highest in the Hin group among the three areas of LLH (Figure 2) ($p < 0.01$). The values of S_R in the upstream zone (Tin) in LLT were obviously higher than those downstream ($p < 0.01$), whereas the result was the inverse in LLH, where the order of S_R value was Hin $<$ Hout $<$ Hmac ($p < 0.01$). In addition, the values of the M and $S_{275-295}$ variation trend were spatially consistent, which were the lowest in the upstream zones (Tin and Hin) and higher in the downstream areas (Tout and Hout). In LLH, the values of M and $S_{275-295}$ were the highest in Hmac ($p < 0.01$) (Table 1).

Significant positive correlations were found between Chla and $a(350)$ in LLT ($R^2 = 0.20$, $p < 0.05$), but there was no remarkably correlative relation in LLH ($R^2 = 0.01$, $p = 0.31$, NS) (Figure 3a). Moreover, there was a significant and positive linear correlation between $a(350)$ and S_R in LLT ($R^2 = 0.21$, $p < 0.01$), whereas a remarkable and negative correlation occurred in LLH ($R^2 = 0.35$, $p < 0.01$) (Figure 3b). Finally, the values of $a(350)$ were negatively correlated with M (LLT: $R^2 = 0.68$, $p < 0.01$; LLH: $R^2 = 0.75$, $p < 0.01$) (Figure 3c) and $S_{275-295}$ (LLT: $R^2 = 0.43$, $p < 0.01$; LLH: $R^2 = 0.71$, $p < 0.01$) (Figure 3d) in LLT and LLH, respectively.

Table 1. Measured nutrient, biological, and optical parameters of water samples summarized as descriptive statistics in the littoral zones of Lakes Taihu and Hongze: All, all sampling sites in LLT or LLH; Tin or Hin, sampling sites of the upstream in LLT or LLH; Tout or Hout sampling sites of the downstream in LLT or LLH; Hmac, sampling sites of zones where aquatic macrophyte dominated and being less affected by rivers in LLH.

| Littoral Zones | Sections | TN (mg/L) | TP (mg/L) | DOC (mg/L) | Chla ($\mu\text{g/L}$) | Secchi Depth (cm) | $S_{275-295}$ (nm^{-1}) | <i>M</i> | <i>S_R</i> |
|-------------------------------------|---------------|--------------------------------------|--------------------------------|---------------------------------|-------------------------------------|-------------------------|--|---------------------------------|--------------------------------|
| LLT Mean \pm SD (Min – Max) | All (n = 91) | 2.06 \pm 0.98 (0.80–5.61) | 0.16 \pm 0.10 (0.05–0.50) | 5.10 \pm 1.62 (2.41–13.29) | 51.06 \pm 47.45 (1.91–279.56) | 60 \pm 30 (25–175) | 0.0195 \pm 0.0026 (0.0157–0.0257) | 8.27 \pm 1.88 (5.54–14.94) | 1.06 \pm 0.14 (0.76–1.45) |
| | Tin (n = 44) | 2.71 \pm 0.92 (0.96–5.61) | 0.21 \pm 0.09 (0.05–0.49) | 4.69 \pm 1.56 (2.41–12.53) | 80.40 \pm 51.06 (8.49–279.56) | 50 \pm 20 (25–110) | 0.0186 \pm 0.0022 (0.0157–0.0239) | 7.19 \pm 1.20 (5.54–11.18) | 1.14 \pm 0.13 (0.93–1.45) |
| | Tout (n = 47) | 1.45 \pm 0.55 (0.80–3.25) | 0.12 \pm 0.08 (0.05–0.50) | 5.49 \pm 1.54 (3.91–13.29) | 23.58 \pm 19.30 (1.92–85.03) | 70 \pm 30 (30–175) | 0.0203 \pm 0.0027 (0.0165–0.0257) | 9.30 \pm 1.83 (6.82–14.94) | 0.98 \pm 0.10 (0.76–1.18) |
| LLH Mean \pm SD (Min – Max) | All (n = 52) | 1.94 \pm 0.81 (0.63–3.15) | 0.22 \pm 0.08 (0.11–0.45) | 5.65 \pm 2.07 (3.92–17.33) | 29.93 \pm 28.23 (2.16–121.10) | 50 \pm 40 (25–180) | 0.0182 \pm 0.0023 (0.0142–0.0230) | 7.63 \pm 1.20 (5.82–10.53) | 1.18 \pm 0.24 (0.88–1.71) |
| | Hin (n = 15) | 2.45 \pm 0.55 (1.44–3.15) | 0.26 \pm 0.07 (0.17–0.45) | 6.81 \pm 3.05 (4.70–17.33) | 13.05 \pm 7.65 (5.26–34.87) | 40 \pm 10 (30–80) | 0.0154 \pm 0.0008 (0.0142–0.0174) | 6.33 \pm 0.30 (5.82–6.83) | 1.05 \pm 0.13 (0.88–1.26) |
| | Hout (n = 19) | 1.88 \pm 0.53 (0.98 \pm 3.02) | 0.23 \pm 0.07 (0.14–0.45) | 4.58 \pm 1.18 (3.00–7.80) | 54.55 \pm 30.93 (10.18–121.10) | 40 \pm 10 (25–80) | 0.0188 \pm 0.0009 (0.0177–0.0212) | 7.86 \pm 0.60 (7.20–9.34) | 1.13 \pm 0.11 (0.99–1.48) |
| | Hmac (n = 18) | 1.32 \pm 0.46 (0.63–2.09) | 0.18 \pm 0.07 (0.11–0.34) | 5.80 \pm 0.80 (3.92–8.21) | 18.01 \pm 15.23 (2.16–53.60) | 80 \pm 50 (30–180) | 0.0198 \pm 0.0021 (0.0151–0.0230) | 8.47 \pm 1.26 (6.28–10.53) | 1.36 \pm 0.31 (0.96–2.35) |

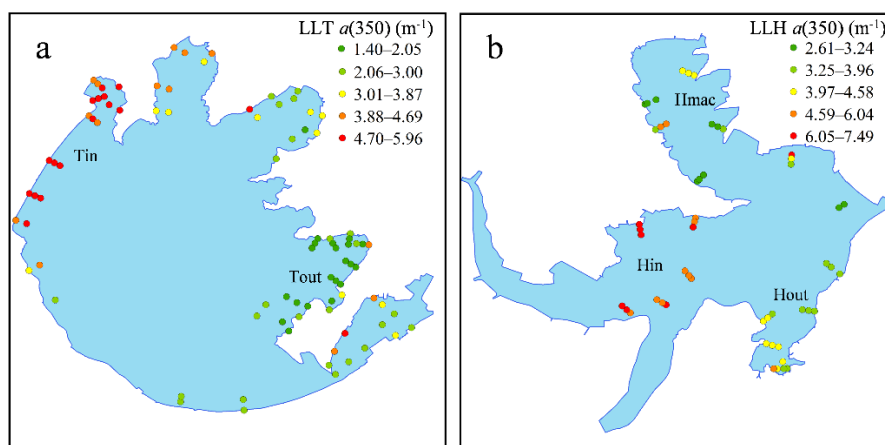


Figure 2. Spatial distribution of $a(350)$ in the littoral zones of Lakes Taihu (a) and Hongze (b).

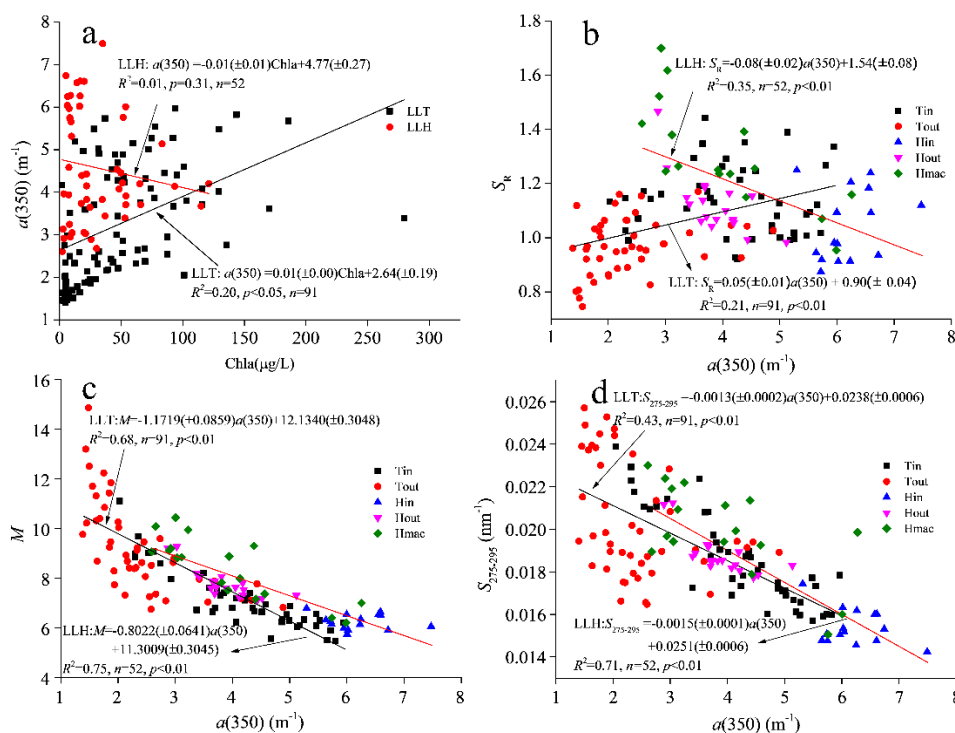


Figure 3. Mutual correlations between CDOM absorption $a(350)$ and Chla (a), S_R (b), the M value (c) and $S_{275-295}$ (d).

3.3. Comparison of Fluorescent CDOM Characteristics

3.3.1. Three-Dimensional Fluorescence Spectra

General characteristics of FDOM can be preliminarily recognized via EEMs spectra using a traditional ‘peak picking’ approach [42], which is intuitive and time-saving, although more in-depth components need to be decomposed using PARAFAC analysis. As shown in Figure 4, two obvious signal peaks of humic-like (Peak C) and protein-like (Peak T) fluorophores appeared in the spectra of water samples in LLT and LLH. Peak C indicates the terrestrial, anthropogenic or agricultural sources, whereas Peak T represents autochthonous origins [43]. Nevertheless the intensities of the fluorescent peaks in LLT and LLH were markedly different; fluorescent EEM spectra in LLT were

mainly dominated by a protein-like fluorophore. In contrast, the primary fluorescent substance type in LLH was humic-like.

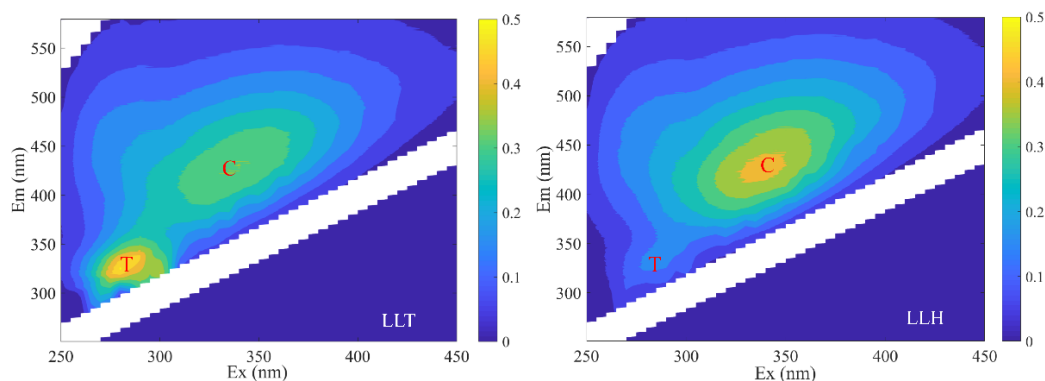


Figure 4. Examples of fluorescent excitation-emission matrix fluorescence spectroscopy (EEMs) spectra from water samples in the littoral zones of Lakes Taihu and Hongze, showing the presence of a humic-like DOM peak (Peak C) and a protein-like DOM peak (Peak T).

3.3.2. Fluorescent Indices Characteristics

The HIX ranged from 0.47 to 1.84 with a mean of 0.80 ± 0.27 in LLT, much lower than that from 2.00 to 5.41 with an average value of 3.68 ± 1.05 in LLH ($p < 0.01$). In addition, the HIX was higher in upstream areas (Tin and Hin) than in the corresponding downstream zones (Tout and Hout) in both LLT and LLH ($p < 0.01$); the HIX value of Hmac was the lowest spatially in LLH ($p < 0.01$) (Figure 5a). The BIX ranged from 0.80 to 1.13 with a mean of 1.00 ± 0.05 in LLT, slightly higher than the range of 0.76 to 0.97 with an average value of 0.85 ± 0.05 in LLH ($p < 0.01$). In addition, the BIX value upstream (Tin) was slightly higher than that downstream (Tout) ($p < 0.05$), whereas the BIX value in LLH was in the order of $Hin < Hout < Hmac$ ($p < 0.05$) (Figure 5b).

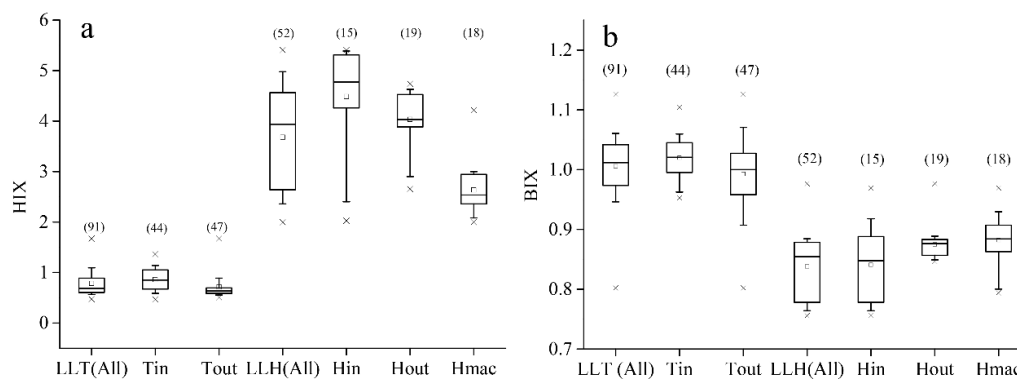


Figure 5. Box plot comparison of the humification index (HIX) and the biological index (BIX) in littoral zones of Lakes Taihu and Hongze: HIX (a); BIX (b). Boxes represent the 25th and 75th percentile; center horizontal line represents the median; square represents the average; whisker ends represent the 10th and 90th percentile; furcation ends represent smallest and largest values; and values in brackets indicate the number of samples.

3.3.3. PARAFAC Components

Four FDOM components of PARAFAC were compared with published PARAFAC models using the OpenFluor online database [44] with excitation and emission similarity score exceeding 0.95 (Figure 6 and Table 2). The EEMs spectral characteristics of C1 were characterized by peaks at 350-nm excitation with 440-nm emission wavelengths, similar to the visible humic-like fluorescent Peak

C and is associated with a group of high molecular weight and aromatic molecules of terrestrial origin [45–48]. C2 was characterized by peaks at 285-nm excitation with 322-nm emission, which is similar to the autochthonous protein-like fluorescent Peak B previously observed and is sensitive to microbial degradation [48–50]. The C3 component had an excitation maximum at 315-nm and emission maximum at 384-nm, similar to the marine humic-like fluorescent Peak M first found in the ocean; this was probably related to microbially derived humic-like [48,49,51,52]. In EEMs spectra of C4, there were two excitation maxima (285 nm and 395 nm) at a 497-nm emission wavelength, only similar to the humic-like fluorescence observed by Kothawala et al. [46], which was unidentified in traditional peaks.

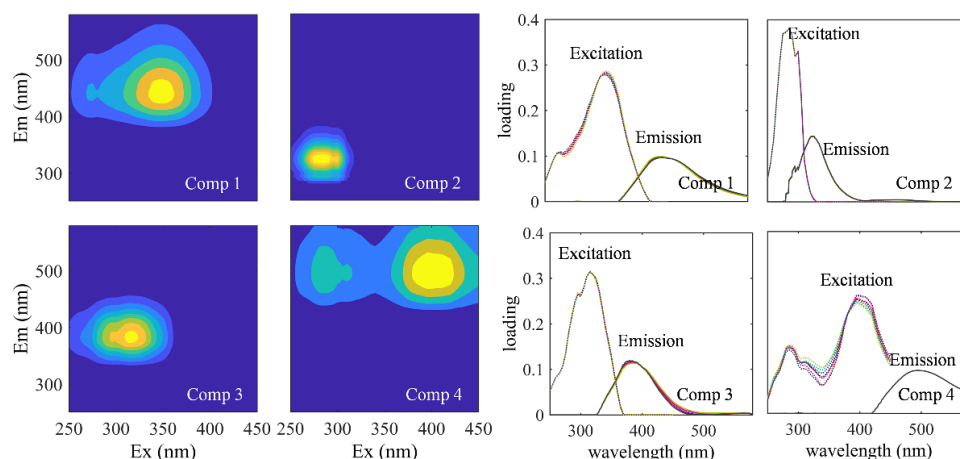


Figure 6. PARAFAC model output showing the fluorescent signatures of the four PARAFAC components in littoral zones of Lakes Taihu and Hongze. Contour plots present the spectral shapes of excitation and emission. Line plots at right side of each contour plot present split-half validation results for the corresponding component and shows the excitation (**left**) and emission (**right**) spectra of six unique split halves and the overall model. For each component these lines are nearly superimposed; the very similar shape of the components provides a nearly perfect validation of the fluorescence signatures.

Table 2. Spectral characteristics of excitation and emission maxima of four fluorescent components identified by PARAFAC analyses compared to the OpenFluor online database.

| Component | Ex _{max} /Em _{max} | Traditional Peak [48] | Description | Number of OpenFluora ^a Matches |
|-----------|--------------------------------------|-----------------------|--|---|
| C1 | 350/440 | Peak C | terrestrial humic-like, high relative aromaticity and molecular weight [45–47] | 12 |
| C2 | 285/322 | Peak B | autochthonous protein-like, sensitive to microbial degradation [49,50] | 2 |
| C3 | 315/384 | Peak M | microbially- derived humic-like [49,51,52] | 6 |
| C4 | (285/395)/497 | No name | unidentified humic-like [46] | 1 |

Note: ^a <http://www.openfluor.org>; test conducted 15 June 2018.

The F_{\max} distribution of each component in LLT and LLH is shown in Figure 7. The F_{\max} values of C1 in LLT were 0.08–0.32 RU with a mean of 0.19 ± 0.07 RU, slightly lower than that in LLH, which ranged from 0.11 RU to 0.42 RU with an average value of 0.27 ± 0.07 RU ($p < 0.01$) (Figure 7a,b). However, it is worth noting that the F_{\max} (C2) concentration in LLT ranged from 0.19 RU to 0.78 RU, significantly higher than that in LLH with a range of 0.05–0.20 RU ($p < 0.01$) (Figure 6c,d). The average value of F_{\max} (C2) of LLT was 0.40 ± 0.12 RU, nearly 4.4 times higher than that of LLH. There was

no significant difference in F_{\max} (C3) between LLT and LLH ($p = 0.06$, NS) (Figure 7e,f). In addition, the F_{\max} (C4) content in LLT was 0.04–0.13 RU with a mean of 0.08 ± 0.03 RU, slightly lower than that in LLH which ranged from 0.05 RU to 0.16 RU with an average of 0.11 ± 0.03 RU ($p < 0.05$) (Figure 7g,h). Because the F_{\max} (C2) markedly increased in LLT, the mean value of the total fluorescent intensity (TFI, sum of F_{\max} values in each sampled water) in LLT was significantly higher than that in LLH ($p < 0.01$).

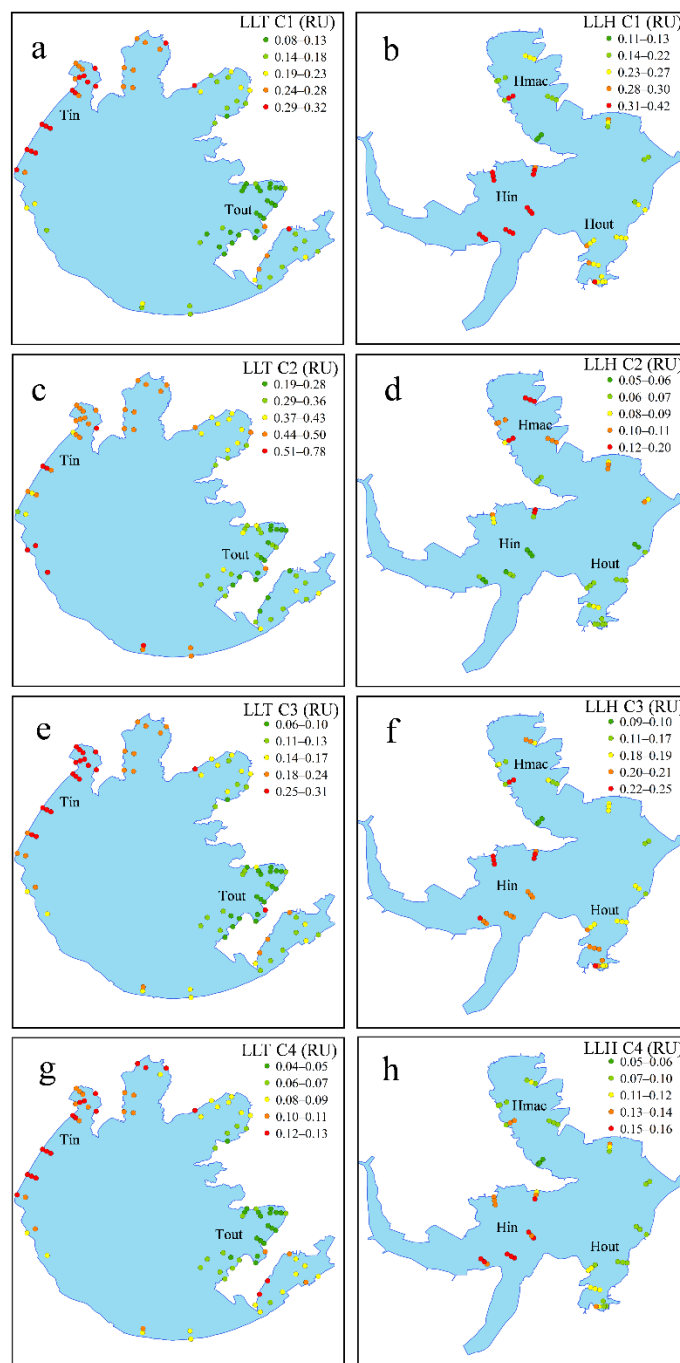


Figure 7. Distribution of each PARAFAC component in littoral zones of Lakes Taihu and Hongze: (a,c,e,g) are C1, C2, C3, and C4 in LLT, respectively, and (b,d,f,h) are the corresponding C1, C2, C3, and C4 in LLH.

Spatially, in LLT, each F_{\max} of four fluorescent components in Tin was significantly higher than that in Tout ($p < 0.01$) (Figure 7). In LLH, each F_{\max} of humic-like substances (C1, C3, and C4) in Hin

was significantly higher than those in Hout and Hmac ($p < 0.01$) (Figure 7). However, there was no significant difference between Hin and Hout in $F_{\max}(\text{C2})$, whereas the $F_{\max}(\text{C2})$ of Hmac was highest among the three sections ($p < 0.01$) (Figure 7).

4. Discussion

4.1. Differences in Sources of FDOM Components in LLT and LLH

It was commonly reported that the sources of C1 and C3 were terrestrial [45–47] and microbially transformed, respectively [49,51,52]. Zhang et al. indicated that rapid increase in $F_{\max}(\text{C3})$ during the phytoplankton degradation experiment [53]; nevertheless there was no significant difference in $F_{\max}(\text{C3})$ between LLT and LLH ($p = 0.06$, NS) (Figure 7e,f), although severe phytoplankton blooms occurred in LLT. What is more, the $F_{\max}(\text{C3})$ had a strong linear correlation to the F_{\max} of terrestrial C1 with high determination coefficients (>0.90) in both LLT and LLH; but no (in LLH) and weak (in LLT) linear correlations with the F_{\max} of autochthonous C2 (Table 3), therefore, we inferred that C3 may be associated with microbial degradation of terrestrial humic-like substance rather than related to algal activities in both LLT and LLH. In addition, it is difficult to illuminate the sources of C4 clearly due to the lack of available and sufficient references due to this component being reported only once; yet it may be photodegradation-related because two excitation peaks consisted of the UVC (290 nm or less) and UVA (339–420 nm) region found in fluorescent signatures, which resulted in it being expected to absorb light, particularly susceptible to UVA due to the majority of UV light of sunlight is UVA light [54].

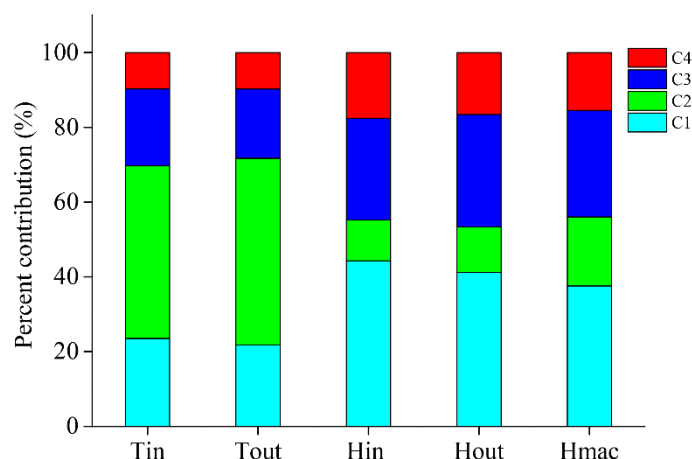
Among the four fluorescent components, the F_{\max} of protein-like C2 contributed greatly majority to the fluorescence intensities in LLT, whereas in LLH, it was dominated by humic-like fluorescent components (Figure 8). Combined with fluorescent EEM spectra (Figure 4), it was concluded that LLT was a protein-like component dominated zone, whereas LLH was a humic-like component dominated zone during the sampling period. A previous study has shown that cyanobacteria in LLT consisted of 40% various proteins (by dry algal weight) [55]. Cyanobacteria degradation releases large amounts of protein substances [56]. Our previous in-situ enclosed experiment also showed that FDOM was dominated by proteinoid materials during a cyanobacterial bloom period [57]. At the same time, S_R may be used as an operational parameter to distinguish between CDOM of different origins. A comparative study indicated that terrestrially derived CDOM had lower S_R [58] and that algal degradation increased S_R [59]. Because the cyanobacterial bloom in LLT caused the increase in S_R in Tin, this resulted in a positive correlation between $a(350)$ and S_R in LLT, but a negative correlation in LLH (Figure 3b), these results were consistent with the previous study of Zhou, et al. [60]. In addition, significant positive correlations were found between Chla and $a(350)$ in LLT, which was also reported by Zhang et al. [53] and Zhou et al. [60] in Lake Taihu, but not in LLH (Figure 3a). All the aforementioned results indicated that frequent cyanobacterial blooms were the main reason for the significant differences in fluorescent components between LLT and LLH.

Moreover, CDOM absorption was highly linearly correlated with the F_{\max} of humic-like C1, C3, and C4, but not (in LLH) or weakly (in LLT) correlated with C2 (Table 3), indicating that CDOM absorption variation was mainly affected by optical humic-like substances, but not or only slightly affected by protein-like components. This explained that although $a(350)$ in LLT was slightly lower than that in LLH, the mean value of TFI in LLT was much higher than that in LLH (Figure 6). This is consistent with the results of Zhang, et al. [61] in Meiliang Bay of Lake Taihu during the summer.

Table 3. Determination coefficients and statistical significance of the linear regression analysis among CDOM absorption and fluorescence intensities of components derived using the PARAFAC model.

| | | LLT | | | | |
|----------------|--|----------------|----------|----------|----------|-------|
| | | <i>a</i> (350) | C1 | C2 | C3 | C4 |
| <i>a</i> (350) | | 1.000 | | | | |
| C1 | | 0.951 ** | 1.000 | | | |
| C2 | | 0.258 * | 0.364 ** | 1.000 | | |
| C3 | | 0.906 ** | 0.966 ** | 0.445 ** | 1.000 | |
| C4 | | 0.941 ** | 0.989 ** | 0.350 ** | 0.940 ** | 1.000 |
| | | LLH | | | | |
| | | <i>a</i> (350) | C1 | C2 | C3 | C4 |
| <i>a</i> (350) | | 1.000 | | | | |
| C1 | | 0.932 ** | 1.000 | | | |
| C2 | | 0.060NS | 0.022NS | 1.000 | | |
| C3 | | 0.806 ** | 0.920 ** | 0.199NS | 1.000 | |
| C4 | | 0.928 ** | 0.981 ** | −0.031NS | 0.940 ** | 1.000 |

Statistical significance was reported as either NS ($p > 0.05$), * ($0.01 < p < 0.05$), or ** ($p < 0.01$).

**Figure 8.** Average contributions to the total CDOM fluorescence intensities (in %) of the four PARAFAC components in the interior section of littoral zones of Lakes Taihu and Hongze. The standard deviation of individual CDOM fluorescence intensity in each section was lower than 10%.

4.2. Differences in Biogeochemical Characteristics of CDOM in LLT and LLH

HIX and BIX have been employed to determine the relative degree of humification and autotrophic productivity of FDOM, respectively [37,62]. In this study, we referred to the division of HIX by Zhang, et al. [63] based on the studies of CDOM in lakes of the Yungui Plateau in China, in which $HIX < 1.5$ indicated a biological or microbial origin, $1.5 < HIX < 2.9$ meant weak humic character and an important recent autochthonous component, $3.0 < HIX < 6.0$ represented a strong humic character and a weak recent autochthonous component, and >6.0 showed a strong humic character and a high terrigenous contribution. As a consequence of the values of HIX in the littoral zones of the two lakes (Figure 5a), the CDOM in LLT had stronger biological characteristics, whereas the FDOM in LLH was mainly affected by the humic character. In comparison to LLH, the CDOM in LLT had a lower degree of relative aromaticity and humification, a higher rate of mineralization and percentage of oxygen-containing functional groups [35]. Higher values of BIX correspond to a stronger autochthonous origin of DOM and higher autotrophic productivity, the lowest values (<1) expound a low abundance of organic matter of biological origin [37,64]. According to the values of the BIX

differences (Figure 5b), in comparison to LLH, the FDOM in LLT had higher autotrophic productivity and a more freshly aquatic bacterial origin.

Furthermore, the M and $S_{275-295}$ values were lower in LLH than those in LLT as a whole ($p < 0.05$) (Table 1), making it clear that the CDOM molecular weight in LLH was higher than that in LLT. Previous study has shown that the majority of terrestrial CDOM has a high molecular weight (HMW) [65]. However, endogenous CDOM substances (phytoplankton-derived) have strong bioavailability, which allowed for transformation of HMW to low molecular weight (LMW) rather easily [53,66].

4.3. CDOM Fates in the Interiors of LLT and LLH

Photochemical reactions and microbial activity often result in CDOM being lost to downstream cycles, and CDOM properties might change significantly during lake water translocation processes [3,67]. $a(350)$ and F_{\max} of the four fluorescent components were higher in the upstream zones (Tin and Hin) than in the downstream zones (Tout and Hout), except there were no significant differences in $F_{\max}(C2)$ between Hin and Hout ($p = 0.95$, NS), and the CDOM depletion rates were higher in LLT than those in LLH (Figures 2 and 7, and Table 4). These results can be attributed to CDOM sources and water hydrology [68,69]. The lake residence time of Lake Taihu is nearly 9 times longer than that in Lake Hongze, which allows CDOM to be more effectively degraded in situ [70,71]. In addition, there was stronger bioavailability of CDOM because of the cyanobacterial bloom in LLT compared to that in LLH, all providing more possibilities for the loss of CDOM in LLT.

In the humic-like components dominated LLH, the endogenous component C2 had no significant loss from upstream (Hin) to downstream (Hout) (Table 4). This may be because of the counteracting effect between the loss during the transportation process and production from phytoplankton, where the Chla of Hout was highest in LLH (Table 1). It is noteworthy that the $F_{\max}(C2)$ of Hmac was highest in LLH, spatially (Figure 7d), because Hmac was dominated by aquatic macrophyte distribution, and a previous study has shown that more protein-like fluorescent substances are produced during macrophyte degradation [61,72]. However, the CDOM release rate from aquatic macrophytes was lower than that from cyanobacteria under the same environmental conditions [61], and aquatic macrophytes did not show obvious degradation during the sampling period, which resulted in aquatic macrophyte-derived CDOM being relatively lower in this study.

Table 4. Differences in mean values of $a(350)$ and F_{\max} of four fluorescent components between upstream and downstream and the corresponding depletion rates in littoral zones of Lakes Taihu and Hongze.

| Parameters | Tin | Tout | Depletion Rate (%) | p Value |
|-----------------------|-------------|-------------|--------------------|---------------|
| $a(350)$ (m^{-1}) | 4.25 ± 1.08 | 2.41 ± 0.85 | 43.25 ± 6.10 | $p < 0.01$ ** |
| $F_{\max}(C1)$ (RU) | 0.25 ± 0.06 | 0.14 ± 0.05 | 45.67 ± 9.84 | $p < 0.01$ ** |
| $F_{\max}(C2)$ (RU) | 0.47 ± 0.09 | 0.33 ± 0.10 | 31.34 ± 11.50 | $p < 0.01$ ** |
| $F_{\max}(C3)$ (RU) | 0.22 ± 0.06 | 0.12 ± 0.05 | 47.77 ± 12.00 | $p < 0.01$ ** |
| $F_{\max}(C4)$ (RU) | 0.10 ± 0.02 | 0.06 ± 0.02 | 41.67 ± 11.79 | $p < 0.01$ ** |
| Parameters | Hin | Hout | Depletion Rate (%) | p Value |
| $a(350)$ (m^{-1}) | 6.07 ± 0.73 | 3.89 ± 0.53 | 35.94 ± 1.01 | $p < 0.01$ ** |
| $F_{\max}(C1)$ (RU) | 0.35 ± 0.03 | 0.25 ± 0.03 | 28.86 ± 5.78 | $p < 0.01$ ** |
| $F_{\max}(C2)$ (RU) | 0.09 ± 0.04 | 0.07 ± 0.01 | \ | $p = 0.95$ NS |
| $F_{\max}(C3)$ (RU) | 0.22 ± 0.02 | 0.18 ± 0.02 | 15.85 ± 3.99 | $p < 0.01$ ** |
| $F_{\max}(C4)$ (RU) | 0.14 ± 0.01 | 0.10 ± 0.01 | 27.93 ± 2.88 | $p < 0.01$ ** |

Statistical significance was reported as either NS ($p > 0.05$) or ** ($p < 0.01$).

The relative molecular weight and humification degree of CDOM decreases as M and $S_{275-295}$ values increase [13,73–75]. $a(350)$ was remarkable linearly negatively correlated with M and $S_{275-295}$ in both LLT and LLH (Figure 3c,d). Therefore, during the changing process from the $a(350)$ -enriched

zone (Tin and Hin) to an $a(350)$ -depleted area (Tout and Hout), the molecular weight and humification degree decreased correspondingly. This also indicated that CDOM shifted from HMW to LMW during the process of CDOM loss. The results of the M and $S_{275-295}$ values as indicative functions of humification were consistent with the consequences of the HIX analysis, which decreased as the humification degree weakened (Figure 5a).

Both Lake Taihu and Lake Hongze are eutrophic shallow lakes in an economically developed eastern coastal region with a large pollutant discharge and a large portion accumulates in the sediment of the littoral zones. As a serious consequence, the sediment release process as result of intense hydrologic processes may be another important factor affecting the characteristics of CDOM in the littoral zones. Further studies of how sediment release affects the CDOM characteristics in the littoral zones of eutrophic shallow lakes need to be performed.

5. Conclusions

This study compared the differences in CDOM characteristics in the littoral zones of eutrophic lake Taihu (LLT, frequently occurring algal blooms and longer lake residence time), and lake Hongze (LLH, no obvious algal blooms and shorter residence time), during the algal season. Four different fluorophores consisting of three humic-like components (C1, C3, and C4) and one protein-like component (C2) were identified. FDOM components were dominated by protein-like fluorescent substances in LLT and by humic-like materials in LLH.

The higher endogenous contribution from the cyanobacterial bloom resulted in the FDOM in LLT having a lower relative molecular weight and aromaticity, humification degree, and higher autotrophic productivity, as compared to LLH. Moreover, the notably longer residence time in LLT resulted in CDOM depletion rates were being higher than those in LLH. In addition, CDOM shifted from HMW to LMW during the CDOM loss process, as the humification degree decreased. This comparative study showed that algal blooms and lake residence time play important roles in the differences in the sources, biogeochemical characteristics, and fates of CDOM in the littoral zones of eutrophic shallow lakes. This work provides field-based knowledge for remote-sensing measurements of CDOM and serves as a reference for lakeshore aquatic environmental management.

Author Contributions: B.C., W.H., and K.C. conceived of the original outline for this study, and designed the sampling points. S.M. and C.L. helped in the data processing and result analysis. M.F. and X.G. performed the analysis with constructive discussions. B.C. wrote the paper. All authors read and approved the final manuscript.

Funding: This research was funded by the State Major Project for Water Pollution Control and Management (No. 2017ZX07603-005), the Major Project for Water Pollution Control of Lake Taihu (No. TH2016401), and the National Natural Science Foundation of China (No. 41673123, No. 41703078 & No. 51409166).

Acknowledgments: We thank Tonghuan Tang, Hui Luo and Yiheng Du for their assistance in water samples collection and determination.

Conflicts of Interest: The authors declare no conflict of interest.

References

1. Zhou, Z.; Guo, L.; Minor, E.C. Characterization of bulk and chromophoric dissolved organic matter in the Laurentian Great Lakes during summer 2013. *J. Great Lakes Res.* **2016**, *42*, 789–801. [[CrossRef](#)]
2. Baker, A.; Coble, P.; Lead, J.; Spencer, R.; Reynolds, D. *Aquatic Organic Matter Fluorescence*; Cambridge University Press: New York, NY, USA, 2014; p. 87, ISBN 978-0-521-76461-2.
3. Zhou, Y.; Zhang, Y.; Shi, K.; Niu, C.; Liu, X.; Duan, H. Lake Taihu, a large, shallow and eutrophic aquatic ecosystem in China serves as a sink for chromophoric dissolved organic matter. *J. Great Lakes Res.* **2015**, *41*, 597–606. [[CrossRef](#)]
4. Gereá, M.; Pérez, G.L.; Unrein, F.; Soto Cárdenas, C.; Morris, D.; Queimaliños, C. CDOM and the underwater light climate in two shallow North Patagonian Lakes: Evaluating the effects on nano and microphytoplankton community structure. *Aquat. Sci.* **2017**, *79*, 231–248. [[CrossRef](#)]

5. Spencer, R.G.M.; Aiken, G.R.; Wickland, K.P.; Striegl, R.G.; Hernes, P.J. Seasonal and spatial variability in dissolved organic matter quantity and composition from the Yukon River basin, Alaska. *Glob. Biogeochem. Cycles* **2008**, *22*, 1–13. [[CrossRef](#)]
6. Patidar, S.K.; Chokshi, K.; George, B.; Bhattacharya, S.; Mishra, S. Dominance of cyanobacterial and cryptophytic assemblage correlated to CDOM at heavy metal contamination sites of Gujarat, India. *Environ. Monit. Assess.* **2015**, *187*, 1–9. [[CrossRef](#)] [[PubMed](#)]
7. Diercks, A.R.; Highsmith, R.C.; Asper, V.L.; Joung, D.J.; Zhou, Z.Z.; Guo, L.D.; Shiller, A.M.; Joye, S.B.; Teske, A.P.; Guinasso, N. Characterization of subsurface polycyclic aromatic hydrocarbons at the Deepwater Horizon site. *Geophys. Res. Lett.* **2010**, *37*, 114–122. [[CrossRef](#)]
8. Gonsior, M.; Schmittkopplin, P.; Stavklint, H.; Richardson, S.D.; Hertkorn, N.; Bastviken, D. Changes in dissolved organic matter during the treatment processes of a drinking water plant in Sweden and formation of previously unknown disinfection byproducts. *Environ. Sci. Technol.* **2014**, *48*, 12714–12722. [[CrossRef](#)] [[PubMed](#)]
9. Miller, R.L.; Mckee, B.A. Using modis terra 250 m imagery to map concentrations of total suspended matter in coastal waters. *Remote Sens. Environ.* **2004**, *93*, 259–266. [[CrossRef](#)]
10. Zhang, Y.; Zhou, Y.; Shi, K.; Qin, B.; Yao, X.; Zhang, Y. Optical properties and composition changes in chromophoric dissolved organic matter along trophic gradients: Implications for monitoring and assessing lake eutrophication. *Water Res.* **2018**, *131*, 255–263. [[CrossRef](#)] [[PubMed](#)]
11. Sharpless, C.M.; Blough, N.V. The importance of charge-transfer interactions in determining chromophoric dissolved organic matter (CDOM) optical and photochemical properties. *Environ. Sci. Process. Impacts* **2014**, *16*, 654–671. [[CrossRef](#)] [[PubMed](#)]
12. Yu, H.; Liang, H.; Qu, F.; Han, Z.S.; Shao, S.; Chang, H.; Li, G. Impact of dataset diversity on accuracy and sensitivity of parallel factor analysis model of dissolved organic matter fluorescence excitation-emission matrix. *Sci. Rep.* **2015**, *5*, 10207. [[CrossRef](#)] [[PubMed](#)]
13. Helms, J.R.; Stubbins, A.; Ritchie, J.D.; Minor, E.C.; Kieber, D.J.; Mopper, K. Absorption spectral slopes and slope ratios as indicators of molecular weight, source, and photobleaching of chromophoric dissolved organic matter. *Limnol. Oceanogr.* **2008**, *53*, 955–969. [[CrossRef](#)]
14. Stedmon, C.A.; Markager, S.; Bro, R. Tracing dissolved organic matter in aquatic environments using a new approach to fluorescence spectroscopy. *Mar. Chem.* **2003**, *82*, 239–254. [[CrossRef](#)]
15. Murphy, K.R.; Stedmon, C.A.; Graeber, D.; Bro, R. Fluorescence spectroscopy and multi-way techniques. *Parafac. Anal. Methods* **2013**, *5*, 6557–6566. [[CrossRef](#)]
16. Mastalerz, M.; Souch, C.; Filippelli, G.M.; Dollar, N.L.; Perkins, S.M. Anthropogenic organic matter in the great marsh of the Indiana dunes national lakeshore and its implications. *Int. J. Coal Geol.* **2001**, *46*, 157–177. [[CrossRef](#)]
17. Zhang, Y.; Yin, Y.; Liu, X.; Shi, Z.; Feng, L.; Liu, M.; Zhu, G.; Gong, Z.; Qin, B. Spatial-seasonal dynamics of chromophoric dissolved organic matter in Lake Taihu, a large eutrophic, shallow lake in China. *Org. Geochem.* **2012**, *42*, 510–519. [[CrossRef](#)]
18. Stets, E.G.S.G.; Cotner, J.B.C.B. Littoral zones as sources of biodegradable dissolved organic carbon in lakes. *Can. J. Fish. Aquat. Sci.* **2008**, *65*, 2454–2460. [[CrossRef](#)]
19. Wang, S.R.; Meng, W.; Jin, X.C.; Zheng, B.H.; Zhang, L.; Xi, H.Y. Ecological security problems of the major key lakes in China. *Environ. Earth Sci.* **2015**, *74*, 3825–3837. [[CrossRef](#)]
20. Cai, Y.; Zhang, Y.; Wu, Z.; Chen, Y.; Xu, J.; Gong, Z. Composition, diversity, and environmental correlates of benthic macroinvertebrate communities in the five largest freshwater lakes of China. *Hydrobiologia* **2017**, *788*, 85–98. [[CrossRef](#)]
21. Xu, H.; Paerl, H.W.; Qin, B.; Zhu, G.; Gao, G. Nitrogen and phosphorus inputs control phytoplankton growth in eutrophic Lake Taihu, China. *Limnol. Oceanogr.* **2010**, *55*, 420–432. [[CrossRef](#)]
22. Zhang, Q. The south-to-north water transfer project of China: Environmental implications and monitoring strategy. *J. Am. Water Resour. Assoc.* **2009**, *45*, 1238–1247. [[CrossRef](#)]
23. Lei, H.; Kai, S.; Jie, B.; Bi, J. Public perception of blue-algae bloom risk in Hongze Lake of China. *Environ. Manag.* **2010**, *45*, 1065–1075.
24. Xu, H.; Paerl, H.W.; Zhu, G.; Qin, B.; Hall, N.S.; Zhu, M. Long-term nutrient trends and harmful cyanobacterial bloom potential in hypertrophic Lake Taihu, China. *Hydrobiologia* **2017**, *787*, 1–14. [[CrossRef](#)]

25. Luo, J.; Li, X.; Ma, R.; Li, F.; Duan, H.; Hu, W.; Qin, B.; Huang, W. Applying remote sensing techniques to monitoring seasonal and interannual changes of aquatic vegetation in Taihu Lake, China. *Ecol. Indic.* **2016**, *60*, 503–513. [[CrossRef](#)]
26. Liu, W.; Deng, W.; Wang, G.; Li, A.; Zhou, J. Aquatic macrophyte status and variation characteristics in the past 50 years in Hongzehu Lake. *J. Hydroecol.* **2009**, *2*, 1–8. (In Chinese)
27. Kowalczuk, P.; Cooper, W.J.; Whitehead, R.F.; Durako, M.J.; Sheldon, W. Characterization of CDOM in an organic-rich river and surrounding coastal ocean in the south Atlantic bight. *Aquat. Sci.* **2003**, *65*, 384–401. [[CrossRef](#)]
28. Cárdenas, C.S.; Gereá, M.; Garcia, P.E.; Pérez, G.L.; Diéguez, M.C.; Rapacioli, R.; Reissig, M.; Queimaliños, C. Interplay between climate and hydrogeomorphic features and their effect on the seasonal variation of dissolved organic matter in shallow temperate lakes of the southern Andes (Patagonia, Argentina): A field study based on optical properties. *Ecohydrology* **2017**, *10*, e1872. [[CrossRef](#)]
29. Markager, S.; Vincent, W.F. Spectral light attenuation and the absorption of UV and blue light in natural waters. *Limnol. Oceanogr.* **2000**, *45*, 642–650. [[CrossRef](#)]
30. Zhou, Y.; Zhang, Y.; Jeppesen, E.; Murphy, K.R.; Shi, K.; Liu, M.; Liu, X.; Zhu, G. Inflow rate-driven changes in the composition and dynamics of chromophoric dissolved organic matter in a large drinking water lake. *Water Res.* **2016**, *100*, 211–221. [[CrossRef](#)] [[PubMed](#)]
31. Zhou, Y.; Zhang, Y.; Shi, K.; Liu, X.; Niu, C. Dynamics of chromophoric dissolved organic matter influenced by hydrological conditions in a large, shallow, and eutrophic lake in China. *Environ. Sci. Pollut. Res.* **2015**, *22*, 12992–13003. [[CrossRef](#)] [[PubMed](#)]
32. Murphy, K.R.; Butler, K.D.; Spencer, R.G.M.; Stedmon, C.A.; Boehme, J.R.; Aiken, G.R. Measurement of dissolved organic matter fluorescence in aquatic environments: An interlaboratory comparison. *Environ. Sci. Technol.* **2010**, *44*, 9405–9412. [[CrossRef](#)] [[PubMed](#)]
33. Lawaetz, A.J.; Stedmon, C.A. Fluorescence intensity calibration using the raman scatter peak of water. *Appl. Spectrosc.* **2009**, *63*, 936–940. [[CrossRef](#)] [[PubMed](#)]
34. Zsolnay, A.; Baigar, E.; Jimenez, M.; Steinweg, B.; Saccomandi, F. Differentiating with fluorescence spectroscopy the sources of dissolved organic matter in soils subjected to drying. *Chemosphere* **1999**, *38*, 45–50. [[CrossRef](#)]
35. Kalbitz, K.; Schmerwitz, J.; Schwesig, D.; Matzner, E. Biodegradation of soil-derived dissolved organic matter as related to its properties. *Geoderma* **2003**, *113*, 273–291. [[CrossRef](#)]
36. Jin, H.; Minhye, P.; Schlautman, M.A. Microbial transformation of dissolved leaf litter organic matter and its effects on selected organic matter operational descriptors. *Environ. Sci. Technol.* **2009**, *43*, 2315–2321.
37. Hugué, A.; Vacher, L.; Relexans, S.; Saubusse, S.; Froidefond, J.M.; Parlanti, E. Properties of fluorescent dissolved organic matter in the gironde estuary. *Org. Geochem.* **2009**, *40*, 706–719. [[CrossRef](#)]
38. Andersson, C.A.; Bro, R. The N-way toolbox for matlab. *Chemom. Intell. Lab. Syst.* **2000**, *52*, 1–4. [[CrossRef](#)]
39. Dillon, P.J.; Rigler, F.H. The phosphorus-chlorophyll relationship in lakes. *Limnol. Oceanogr.* **1974**, *19*, 767–773. [[CrossRef](#)]
40. Ebina, J.; Tsutsui, T.; Shirai, T. Simultaneous determination of total nitrogen and total phosphorus in water using peroxodisulfate oxidation. *Water Res.* **1983**, *17*, 1721–1726. [[CrossRef](#)]
41. Kozak, A.; Kowalczevska-Madura, K.; Gołdyn, R.; Czart, A. Phytoplankton composition and physicochemical properties in Lake Swarzędzkie (midwestern Poland) during restoration: Preliminary results. *Arch. Pol. Fish.* **2014**, *22*, 17–28. [[CrossRef](#)]
42. Fellman, J.B.; Hood, E.; Spencer, R.G.M. Fluorescence spectroscopy opens new windows into dissolved organic matter dynamics in freshwater ecosystems: A review. *Limnol. Oceanogr.* **2010**, *55*, 2452–2462. [[CrossRef](#)]
43. Coble, P.G. Marine optical biogeochemistry: The chemistry of ocean color. *Chem. Rev.* **2007**, *107*, 402–418. [[CrossRef](#)] [[PubMed](#)]
44. Murphy, K.R.; Stedmon, C.A.; Wenig, P.; Bro, R. Openfluor- an online spectral library of auto-fluorescence by organic compounds in the environment. *Anal. Methods* **2014**, *6*, 658–661. [[CrossRef](#)]
45. Lambert, T.; Bouillon, S.; Darchambeau, F.; Morana, C.; Roland, F.A.E.; Descy, J.P.; Borges, A.V. Effects of human land use on the terrestrial and aquatic sources of fluvial organic matter in a temperate river basin (the Meuse river, Belgium). *Biogeochemistry* **2017**, *136*, 191–211. [[CrossRef](#)]

46. Kothawala, D.N.; Wachenfeldt, E.V.; Koehler, B.; Tranvik, L.J. Selective loss and preservation of lake water dissolved organic matter fluorescence during long-term dark incubations. *Sci. Total Environ.* **2012**, *433*, 238–246. [[CrossRef](#)] [[PubMed](#)]
47. Lambert, T.; Bouillon, S.; Darchambeau, F.; Massicotte, P.; Borges, A.V. Shift in the chemical composition of dissolved organic matter in the Congo River network. *Biogeosciences* **2016**, *13*, 5405–5420. [[CrossRef](#)]
48. Coble, P.G. Characterization of marine and terrestrial DOM in seawater using excitation-emission matrix spectroscopy. *Mar. Chem.* **1996**, *51*, 325–346. [[CrossRef](#)]
49. Osburn, C.L.; Wigdahl, C.R.; Fritz, S.C.; Saros, J.E. Dissolved organic matter composition and photoreactivity in prairie lakes of the U.S. Great plains. *Limnol. Oceanogr.* **2011**, *56*, 2371–2390. [[CrossRef](#)]
50. Li, P.; Chen, L.; Zhang, W.; Huang, Q. Spatiotemporal distribution, sources, and photobleaching imprint of dissolved organic matter in the Yangtze estuary and its adjacent sea using fluorescence and parallel factor analysis. *PLOS ONE* **2015**, *10*, e0130852. [[CrossRef](#)] [[PubMed](#)]
51. Lapiere, J.F.; Del Giorgio, P.A. Partial coupling and differential regulation of biologically and photochemically labile dissolved organic carbon across boreal aquatic networks. *Biogeosciences* **2014**, *11*, 5969–5985. [[CrossRef](#)]
52. Murphy, K.R.; Stedmon, C.A.; Waite, T.D.; Ruiz, G.M. Distinguishing between terrestrial and autochthonous organic matter sources in marine environments using fluorescence spectroscopy. *Mar. Chem.* **2008**, *108*, 40–58. [[CrossRef](#)]
53. Zhang, Y.; Dijk, M.A.; Liu, M.; Zhu, G.; Qin, B. The contribution of phytoplankton degradation to chromophoric dissolved organic matter (CDOM) in eutrophic shallow lakes: Field and experimental evidence. *Water Res.* **2009**, *43*, 4685–4697. [[CrossRef](#)] [[PubMed](#)]
54. Ishii, S.K.; Boyer, T.H. Behavior of reoccurring parafac components in fluorescent dissolved organic matter in natural and engineered systems: A critical review. *Environ. Sci. Technol.* **2012**, *46*, 2006–2017. [[CrossRef](#)] [[PubMed](#)]
55. Li, K. The Feasibility Study on the Use of Cyanobacteria of Taihu Lake. Master's Thesis, Jiangnan University, Wuxi, China, 2009. (In Chinese)
56. Henderson, R.K.; Baker, A.; Parsons, S.A.; Jefferson, B. Characterisation of algogenic organic matter extracted from cyanobacteria, green algae and diatoms. *Water Res.* **2008**, *42*, 3435–3445. [[CrossRef](#)] [[PubMed](#)]
57. Chen, B.; Feng, M.; Shang, L.; Ke, F.; Wu, X.; Li, Y. Effects on cyanobacterial growth and water quality after harvesting accumulated cyanobacteria in autumn: An in-situ experiment in Lake Chaohu. *J. Lake Sci.* **2016**, *28*, 253–262. (In Chinese)
58. Chen, H.; Zheng, B.; Song, Y.; Qin, Y. Correlation between molecular absorption spectral slope ratios and fluorescence humification indices in characterizing CDOM. *Aquat. Sci.* **2011**, *73*, 103–112. [[CrossRef](#)]
59. Chen, B. Research on Characteristic Variations and the Controll of Contaminants from Accumulative Blue-Green Algae in Lakeshore. Master's Thesis, Suzhou University of Science and Technology, Suzhou, China, 2015. (In Chinese)
60. Zhou, Y.; Jeppesen, E.; Zhang, Y.; Niu, C.; Shi, K.; Liu, X.; Zhu, G.; Qin, B. Chromophoric dissolved organic matter of black waters in a highly eutrophic chinese lake: freshly produced from algal scums? *J. Hazard. Mater.* **2015**, *299*, 222–230. [[CrossRef](#)] [[PubMed](#)]
61. Zhang, Y.; Liu, X.; Wang, M.; Qin, B. Compositional differences of chromophoric dissolved organic matter derived from phytoplankton and macrophytes. *Org. Geochem.* **2013**, *55*, 26–37. [[CrossRef](#)]
62. Yang, L.; Zhuang, W.; Chen, C.; Wang, B.; Kuo, F. Unveiling the transformation and bioavailability of dissolved organic matter in contrasting hydrothermal vents using fluorescence EEM-PARAFAC. *Water Res.* **2017**, *111*, 195–203. [[CrossRef](#)] [[PubMed](#)]
63. Zhang, Y.; Zhang, E.; Yin, Y.; Dijk, M.A.V.; Feng, L.; Shi, Z.; Liu, M.; Qina, B. Characteristics and sources of chromophoric dissolved organic matter in lakes of the Yungui plateau, China, differing in trophic state and altitude. *Limnol. Oceanogr.* **2010**, *55*, 2645–2659. [[CrossRef](#)]
64. Para, J.; Coble, P.G.; Charrière, B.; Tedetti, M.; Fontana, C.; Sempéré, R. Fluorescence and absorption properties of chromophoric dissolved organic matter (CDOM) in coastal surface waters of the northwestern Mediterranean sea, influence of the Rhône river. *Biogeosciences* **2010**, *7*, 4083–4103. [[CrossRef](#)]
65. Berggren, M.; Ström, L.; Laudon, H.; Karlsson, J.; Jonsson, A.; Giesler, R.; Bergström, A.; Jansson, M. Lake secondary production fueled by rapid transfer of low molecular weight organic carbon from terrestrial sources to aquatic consumers. *Ecol. Lett.* **2010**, *13*, 870–880. [[CrossRef](#)] [[PubMed](#)]

66. Nguyen, M.L.; Hu, Q.; Sommerfeld, M.; Westerhoff, P.; Baker, L.; Esparzasoto, M. Characteristics and reactivity of algae-produced dissolved organic carbon. *J. Environ. Eng.* **2005**, *131*, 1574–1582. [[CrossRef](#)]
67. Hood, E.; Fellman, J.; Spencer, R.G.; Hernes, P.J.; Edwards, R.; D'Amore, D.; Scott, D. Glaciers as a source of ancient and labile organic matter to the marine environment. *Nature* **2009**, *462*, 1044–1047. [[CrossRef](#)] [[PubMed](#)]
68. Goodman, K.J.; Baker, M.A.; Wurtsbaugh, W.A. Lakes as buffers of stream dissolved organic matter (DOM) variability: Temporal patterns of DOM characteristics in mountain stream-lake systems. *J. Geophys. Res. Biogeosci.* **2011**, *116*, 178–181. [[CrossRef](#)]
69. Chen, Y.; Yu, K.; Zhou, Y.; Ren, L.; Kirumba, G.; Zhang, B.; He, Y. Characterizing spatiotemporal variations of chromophoric dissolved organic matter in headwater catchment of a key drinking water source in China. *Environ. Sci. Pollut. Res. Int.* **2017**, *24*, 27799–27812. [[CrossRef](#)] [[PubMed](#)]
70. Dillon, P.J.; Molot, L.A. Dissolved organic and inorganic carbon mass balances in central Ontario lakes. *Biogeochemistry* **1997**, *36*, 29–42. [[CrossRef](#)]
71. Schindler, D.W. Lakes as sentinels and integrators for the effects of climate change on watersheds, airsheds, and landscapes. *Limnol. Oceanogr.* **2009**, *54*, 2349–2358. [[CrossRef](#)]
72. Yao, X.; Zhang, Y.; Zhu, G.; Qin, B. Different degradation mechanism of dissolved organic matter derived from phytoplankton and macrophytes in Lake Taihu, China. *Acta Sci. Circumst.* **2014**, *34*, 688–694. (In Chinese)
73. Uyguner, C.S.; Bekbolet, M. Implementation of spectroscopic parameters for practical monitoring of natural organic matter. *Desalination* **2005**, *176*, 47–55. [[CrossRef](#)]
74. Peuravuori, J.; Pihlaja, K. Molecular size distribution and spectroscopic properties of aquatic humic substances. *Anal. Chim. Acta* **1997**, *337*, 133–149. [[CrossRef](#)]
75. Li, S.; Zhang, J.; Mu, G.; Ju, H.; Wang, R.; Li, D. Spatiotemporal characterization of chromophoric dissolved organic matter (CDOM) and CDOM-DOC relationships for highly-polluted river. *Water* **2016**, *8*, 399. [[CrossRef](#)]



© 2018 by the authors. Licensee MDPI, Basel, Switzerland. This article is an open access article distributed under the terms and conditions of the Creative Commons Attribution (CC BY) license (<http://creativecommons.org/licenses/by/4.0/>).